Single Event Upsets in Implantable Cardioverter Defibrillators

P.D. Bradley[1] and E. Normand[2]

[1] Department of Engineering Physics, University of Wollongong, 2522, Wollongong, Australia.

[2] Boeing Defense and Space Group, Seattle, WA 98124-2499 USA

Abstract

Single event upsets (SEU) have been observed in implantable cardiac defibrillators. The incidence of SEUs is well modeled by upset rate calculations attributable to the secondary cosmic ray neutron flux. The effect of recent interpretations of the shape of the heavy ion cross-section curve on neutron burst generation rate calculations is discussed. The model correlates well with clinical experience and is consistent with the expected geographical variation of the secondary cosmic ray neutron flux. The observed SER was 9.3×10^{-12} upsets/bit-hr from 22 upsets collected over a total of 284672 device days. This is the first clinical data set obtained indicating the effects of cosmic radiation on implantable devices. Importantly, it may be used to predict the susceptibility of future implantable device designs to cosmic radiation. The significance of cosmic radiation effects relative to other radiation sources applicable to implantable devices is discussed.

I. Introduction

Approximately 350000 to 450000 individuals suffer an episode of out-of-hospital cardiac arrest every year in the United States, with less than 25% surviving the first episode. It has been demonstrated that if sudden death survivors are untreated the recurrence rate is extremely high, with an annual sudden death mortality of 30% [1] .

The Implantable Cardiac Defibrillator (ICD) emerged in the early 1990s as the "gold-standard therapy" for sudden cardiac death survivors. The original concept of the ICD is attributed to Dr. Michel Mirowski [2] in the mid 1960s. He recognized the utility of permanently implanting a device which automatically detects the high rate condition associated with ventricular fibrillation and delivers a high energy shock to the heart to restore the sinus (normal) rhythm. The high energy shock (up to 700V, 30 Joules) simultaneously depolarizes the entire myocardium (heart muscle) and effectively interrupts the chaotic circular current patterns associated with fibrillation. The first human implant occurred in 1980.

In common with the space electronics industry, design criteria include low power consumption, high longevity, high reliability and small size. Despite the trend towards devices with smaller critical charges and the increasing sophistication and use of MOS devices in medical products, there have been no earlier reported cases of single event upsets in medical devices. Previous reports on the susceptibility of implantable medical devices to ionizing radiation only considered total dose effects. [e.g. 3,4].

This paper initially presents a brief review of the sources of radiation relevant to implantable medical devices. The review considers both total dose and transient effects with the aim of determining the relative significance of various sources. The remainder of the paper examines terrestrial cosmic ray single event upset models and their applicability to implantable medical devices. The models are then compared with ICD clinical experience.

II. Summary of Ionizing Radiation Effects on Implantable Devices

Ionizing radiation effects on MOS electronics may be classed into two broad categories [5]:

Total Ionizing Dose Effects (TID) due to charge accumulation in oxide regions: Threshold voltage changes have been seen at around 10 Gy [6] whilst degradation in the isolation between and within n-channel devices may occur at relatively low radiation levels (10-50 Gy) [5]. From these results, it would appear that a reasonable lower bound on the sensitivity of MOS electronics is approximately 10 Gy.

Single Event Effects (SEE) due to high LET particles depositing sufficient charge to perturb circuit operation: We only need to consider single event upset due to alpha particles from the device packaging and high energy neutrons from cosmic radiation or radiotherapy. Other single effects such as single event latch-up, burnout and gate rupture of power MOSFETs have negligible probability of occurrence. Normand [7] states that only a small number of MOS parts are prone to neutron/proton induced latch-up and even if a device is susceptible, the latch-up rate per device is much lower then the single event upset rate by several orders of magnitude. Gate rupture requires very high energy ions not applicable to a medical device [7]. Single event burnout (SEB) [7,8] of an N-channel power MOSFET is possible in high voltage rated parts operating at high drain to source voltages. The implantable cardiac defibrillator has components with a very large voltage rating (>1000V). However, the required biasing conditions for susceptibility are only rarely present (e.g. during charging of the device for shock therapy) and thus the device is not considered susceptible to SEB. The authors do not know of any implantable medical device with the required MOSFETs operating continuously at high drain to source voltages. It would appear that SEB is not a real issue for current implantable medical devices.

Table 1 lists all the main ionizing radiation sources applicable to implantable devices. Radiation sources that may adversely affect implanted electronics (dose greater than 10 Gy or have SEU potential) are underlined in comments.

Table 1.
Summary of radiation sources applicable to implantable devices

Source	Radiation	Dose	Comments
Natural [9]			
External Irradiation: Cosmic Rays	p,β, n, pion, muon	0.28 mGy(Lung)	Secondary neutrons may cause SEU
Terrestrial Radiation	α,β,γ	0.32 mGy(Lung)	
Internal Irradiation: Radionuclides (e.g. K40)	α,β,γ	0.50 mGy(Lung)	
Electronic Packaging TraceUranium/Thorium	α	low dose, E<10MeV	May cause SEU.
Diagnostic/Nuclear Medicine [9,10,11,12]		Average Doses/test	
Thyroid Scan (^{131}I Radionuclide)	γ (360,640 keV)β^-	500 mGy(Thyroid)	
Lung Scan (^{99m}Tc Radionuclide)	γ (140keV)	60 mGy(Thyroid)	
Single Photon Emission Computed Tomography (SPECT)	As above	Slightly > than above planar scan	
Positron Emission Tomography (PET)	β^-,β^+	tens of mGy	
In-vivo neutron activation analysis (PuBe) [28]	n, γ,various others	relatively low.	Neutron SEU(device Qc<0.15pC)
Diagnostic/X-ray techniques			
Fluoroscopy (Pacemaker Insertion) [13]	X-Ray<200keV	1300 mGy (Skin)	
Fluoroscopy (Coronary Angioplasty)	X-Ray<200keV	1000-5000 mGy (Skin)	
Computed Tomography	X-Ray<200keV	50-140 mGy (Tissue)	
Radiographic Chest Examinations	X-Ray<200keV	0.2mGy(Entrance)	
Therapeutic/Nuclear Medicine [10,14]			
Thyroid Cancer (^{131}I Radionuclide)	γ (360,640 keV) β^- (610 keV)	40Gy(Thyroid) 0.7Gy(gonad)	Assuming 5000Mbq. Dose/activity from [9]
Therapeutic/External Beam, Sealed Source		Target Absorbed Doses	
Teletherapy (Breast)	>1MeV γ and β	50 (30-60) Gy	Total dose, SEU due to photo-disintegration neutrons
Teletherapy (Lung/Thorax)	>1MeV γ and β	60 (20-60) Gy	
Proton or Fast Neutron therapy	p, n	Expt. Treatment	Total dose ,possible SEU
Heavy Ion Therapy	Heavy Ion	Expt. Treatment	Total dose, possible SEU
Boron Neutron Capture Therapy	n, α	Expt. Treatment	Total dose ,possible SEU

Note: Radiation sources which may adversely affect implanted electronics, that is, have a dose greater than 10 Gy or have SEU potential, are underlined in comments. Teletherapy is a general term referring to LINAC or ^{60}Co external treatment.

The only radiation source which may generate total dose effects in implantable medical devices is radiotherapy in which up to 70 Gy of 1-20 MeV gamma or beta radiation may be delivered to a tumor site. Several studies have confirmed the sensitivity of CMOS based pacemakers and ICDs to therapeutic doses of radiation. A comprehensive review of the literature has recently been compiled by Bradley [15]. To assess the magnitude of the problem, it was estimated that of approximately 2 million people implanted worldwide with pacemakers, around 1800 per year will require radiotherapy in the chest region [15]. Currently, implant device manufacturers label products warning against such irradiation. Several options exist for such irradiation; the device may be temporarily explanted or irradiation may proceed with appropriate shielding designed to reduce the pacemaker dose to less than around 10 Gy with the device operation continuously monitored.

Unlike total dose effects, single event effects, due to high-energy neutrons from cosmic radiation or alpha particles emitted from the die packaging, are ubiquitous. In this sense, their significance to device reliability is potentially of much greater importance. SEUs due to packaging alphas have been effectively eliminated in three ways:

1. Improved quality control on the raw materials used in the manufacturing process,
2. Applying a coating (polyimide or silicone) over the die to completely shield out the alpha particles and
3. For DRAMs, in some cases, introducing a minority carrier barrier below the cell capacitor [16].

Of the three methods, the quality control measures used to screen raw materials for low alpha concentrations has been the most effective. Shielding is not practical for cosmic ray secondary neutrons. The relatively low incidence of therapeutic radiation incident on an implantable device and the elimination of incident alpha particles leaves *cosmic radiation induced secondary neutron single event upset (SEU) as the main pervasive ionizing radiation threat to the reliability of implantable devices.* The most sensitive circuit structure within typical microcomputer architectures is the RAM due to the small amount of charge used to store information. Those systems in which critical controlling software is in RAM, as opposed to ROM (Read Only Memory), are especially prone

to SEUs. In this study, we neglect microprocessor SEE since we assume that the critical charge associated with microprocessor circuit elements is much higher than the RAM.

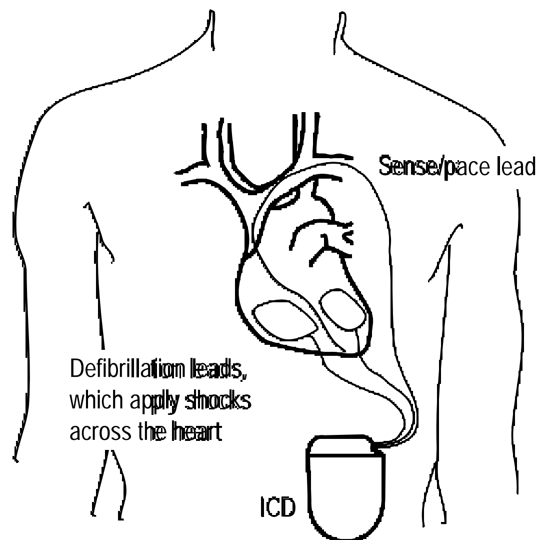

Figure 1: ICD Implant with patch leads

III. Brief Description of ICD and RAM

The ICD typically consists of a pacemaker which senses and paces (if necessary) the heart via one or two sensing leads connected to the epicardium or transvenously to the endocardium. A defibrillating lead system may be attached to the heart using large patch electrodes on the epicardium or by using a transvenous endocardial system. The device is hermetically sealed in a titanium case which houses the pacemaker and defibrillator electronics, high voltage inverter circuitry with large shock delivery capacitors (120 μF) and a high density battery (Lithium silver vanadium oxide). The device is implanted in a left sub-pectoral position or subcutaneously in the left abdominal region. Typical lead and implant positions are shown in Figure 1.

Device electronic architecture varies from one manufacturer to another. Three models of ICDs from the one manufacturer are used in this study. The models span several generations of development as device size is reduced and new therapy modalities and features have been introduced. However, all three models share a common 32K×8 bit resistive load NMOS RAM integrated circuit embedded in similar microcomputer architectures. The RAM is a critical component for device operation since it is used for storage of program code and data. Details of the RAM considered in this study are provided in Table 2. Note that the RAM uses a silicone rubber die coating to eliminate alpha particles emanating from the packaging. This is very rare in 1990s vintage RAMs.

IV. Modeling Cosmic Ray Secondary Neutron Upset Rates in ICDs

An SEU may occur when a high energy neutron strikes the reversed biased p-n junction of a memory cell and deposits sufficient charge to cause a change in memory state. The region in which the charge must be deposited is defined as the sensitive volume (V) and the amount of charge required to just cause an SEU is called the critical charge (Q_C).

Table 2.
Data for the 32K×8 bit SRAM Die

Parameter	Value
Organization	32K words by 8 bits 262144 bits
Die Size[17]	4.98 mm × 9.16 mm: 45.62 mm^2
Cell Size[17]	7.4 μm × 12.8 μm: 94.72 μm^2
Address Map	See Appendix I of [15]
Feature Size[17]	1.3 μm
Gate Length[17]	1.2 μm
Gate Oxide Thickness (t_{ox}) [17,18]	25 nm
Field Oxide Thickness[18]	500 nm
N+ Diffusion Depth[18]	0.28 μm
P+ Diffusion Depth[18]	0.32 μm
P Well Depth[18]	3.75 μm
Heavy Ion Test Data[18,19,20,21]	Figure 2
Proton Test Data[18,21]	

Note: Geometry data from Harboe-Sorensen [18] originally obtained by reverse engineering work performed at the National Microelectronics Center, Ireland.

High energy neutrons are a major component of the terrestrial cosmic radiation spectra. The required charge deposition for upset may be generated by elastic or inelastic scattering in the silicon ($Si<n,n>Si$ reaction). For elastic scattering, the kinetic energy transferred from the neutron causes a short range recoil (a few microns) of the substrate nucleus. The rapidly decelerating recoil, a Si ion, deposits considerable charge in a small volume generating a large number of electron-hole-pairs. Alternatively, if the energy of the neutron is above a certain threshold value, a proton ($Si^{28}<n,p>Al^{28}$ reaction, Q=-7.714MeV) or an alpha particle($Si^{28}<n,\alpha>Mg^{25}$ reaction, Q=-2.654MeV) may escape from the silicon nucleus. In this case, both the recoil nucleus and the light particle will generate a large number of electron-hole pairs.

Normand [22] proposes two main methods of calculating SEU rates in avionics. Such methods may also be applied to terrestrial conditions by suitable consideration of the variation in neutron flux.

A. *Upset Rate by the Burst Generation Method*

1. *Basic Burst Generation Rate Model:*

The burst generation rate (BGR) method for predicting SEU rates in integrated circuits was first proposed by Ziegler and Lanford [23] and subsequently refined by several groups [24]-[28]. In the BGR method, the atmospheric soft error rate (SER) is given by

$$SER = C(E_r, t)\ Sf\ V \int_{En} BGR(E_n, E_r) \frac{dN}{dE_n} dE_n \quad (1)$$

where $C(E_r,t)$ is the collection efficiency which accounts for the escape of nuclear recoils from the sensitive volume V having a mean thickness t, Sf is a shielding factor to account for ground level neutrons attenuation due to buildings and tissue, dN/dE_n is the differential atmospheric neutron flux spectra and $BGR(E_n,E_r)$ is the burst generation rate($cm^2/\mu m^3$) spectra defined as the partial macroscopic cross section for producing silicon recoils with energy greater than the minimum necessary recoil energy (E_r) times the atomic density of silicon (5×10^{10} /μm^3). Since it requires 3.6 eV to generate an electron hole pair in silicon then the minimum recoil energy is given by

$$E_r(in\ MeV) = Qc(in\ pC) \times 22.5 \quad (2)$$

The function obtained by integrating the product of the neutron energy spectrum and the BGR over all recoil energies E> E_r is called the Neutron Induced Error (NIE in $cm^2/\mu m^3$). It gives the number of errors induced by a unit fluence of neutrons (1 cm^{-2}) in a unit volume of silicon (1 μm^3). Eqn (1) then simplifies to

$$SER = C(Qc, t)\ Sf\ V\ F\ NIE(Qc) \quad (3)$$

where F is the integral neutron flux($cm^{-2}s^{-1}$) greater than 1 MeV. Two main assumptions exist in the above model; the NIE function and BGR function assume point deposition of charge and we assume negligible energy loss of recoils (eqn (2)) due to heat production. The first assumption is accounted for by the collection efficiency term whilst heat production is only important for low energy ions (<a few MeV) and may be ignored for critical charges above about 50fC [29].

2. Estimation of Qc, V and t and the Interpretation of the Heavy Ion Cross-Section Curve:

Previous calculations [43] in the literature have assumed critical charge is variable across the memory array requiring a modification of eqn (3). The distribution of critical charge was assumed to be characterized by heavy ion upset test data. A four-parameter integral Weibull distribution is generally used to model the cross-section as given by

$$cs(L) = cs0\left(1 - e^{-[(L-L0)/W]^s}\right) \quad L \geq L0 \quad (4)$$
$$= 0 \quad L < L0$$

where L0 is the threshold(in MeV/(mg/cm^2)), W is the width of the distribution (in MeV/(mg/cm^2)), s is a shape parameter and cs0 is the limiting cross-section (or sensitive area in cm^2/device or cm^2/bit). These parameters were obtained by fitting eqn (4) to heavy ion test data [18,21] with the results given in Table 4 and Figure 2.

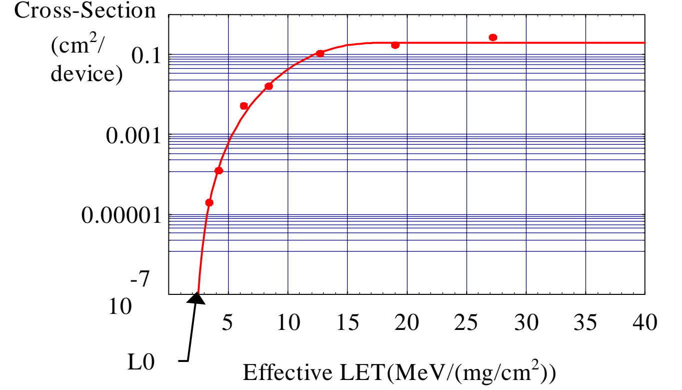

Figure 2: Heavy-Ion testing cross-section curve

Assuming that cell to cell variations in critical charge are responsible for the shape of the heavy ion curve and that the sensitive volume is well represented by an RPP geometry it follows that SER may be calculated as

$$SER = Sf\ t\ F \int_{L0}^{\infty} C(Qc(L,t),t) NIE(Qc(L,t)) \frac{dcs(L)}{dL} dL \quad (5)$$

where $Qc = 0.01Lt$

However, a thorough review of the interpretation of heavy ion data was recently performed by Petersen [30]. The width and shape of the heavy ion curve was found to be predominantly determined by intra-cell variations of charge collection and not by cell to cell variations. A fixed critical charge is then appropriate for BGR SEU calculations. Petersen initially suggested [30] that the heavy ion curve describes the variation in effective path length with varying LET. The heavy ion cross-section may then be used to extract the shape of the sensitive volume. This approach has the disadvantage that a charge collection depth that includes charge amplification or diffusion may be physically incompatible with geometrical limitations in the path [31]. Subsequently the concept of a charge collection gain was introduced to account for the variation in cross-section. A constant depth is then assumed.

The SER using the charge collection gain concept may then be calculated using

$$SER = Sf\ t\ F \int_{L0/L50}^{\infty} C(aQcf(t),t) NIE(aQcf(t)) \frac{dcs(a)}{da} da \quad (6)$$

where $Qcf = 0.01 L_{50} t$ and $a = L / L_{50}$

L_{50} is the median LET corresponding to 50% of the limiting cross-section and Qcf is the fixed critical charge defined at that point. We define an attenuation factor (a) that is the inverse of Petersen's collection gain [31]. The critical charge is scaled by the collection attenuation. An area with a low attenuation (e.g. high gain charge amplification) will effectively require a smaller deposited charge for upset. Conversely, a region with a high attenuation (e.g. diffusion point removed from junction) will require a higher deposited charge for upset. One may think of the cross-section as describing the variation in effective critical charge ($aQcf$) within a single cell. Comparison of equations (5) and (6) show they are identical. A variation in gain within a cell is mathematically equivalent to a variation in critical charge across the entire device. This is

an important result since it indicates that previous BGR calculations, based on assuming cell to cell variations in critical charge, provide the correct result when current interpretations are applied.

In this work, we calculate the SER using two methods:

1. Collection gain variation model: RPP geometry with constant depth. Eqn (6) calculates SER.
2. Sensitive depth variation model: Sensitive volume shape extracted from heavy ion data. Eqn (3) calculates SER.

Comparing models tests the effect of a varying sensitive depth. The ideal probably lies somewhere between the two models with the heavy ion curve affected by both sensitive depth and collection gain variations. Since Qc is constant, we may define

$$Qc = 0.01Lt = 0.01L0\,t_{\max} = 0.01\bar{L}\,\bar{t} \tag{7}$$

where t_{max} is the maximum sensitive volume depth (for sensitive depth variation model) and $\bar{t}$ is the mean depth.

Two approaches are possible to determine Qc and $\bar{t}$:

1. Qc may be determined from circuit analysis methods [32]. All other parameters are defined by fitting heavy ion data to eqn (4) with sensitive depth calculated from eqn (7).
2. The expected mean sensitive depth ($\bar{t}$) may be estimated from charge collection spectroscopy methods developed by McNulty [33] or using the depth of the depletion region corrected for drift funneling and diffusion effects [34,35]. All other parameters are defined by fitting heavy ion data to eqn (4) with Qc calculated from eqn (7).

Of these two approaches, we use the second since circuit analysis data was not available to apply the first approach. It was assumed that the sensitive depth would be limited by a p-well potential barrier typically employed in the design of resistive load NMOS devices for SER improvement. It was thus assumed that $\bar{t}$ would be limited to about one half of the depth of the quasi-neutral region in the p-well. The expected mean sensitive depth ($\bar{t}$) was estimated at 2.2µm taking into account the p-well potential barrier and using the depletion depth and funnel equation of Hu [34]. The final values obtained are summarized in Table 4.

3. Voltage dependency of parameters

Of importance in this analysis is an examination of key parameter variation with supply voltage (Vdd) since test data is obtained at 5V but the device operating voltage is 2.8V.

Sensitive Volume: The sensitive depth is predominantly determined by the p-well potential barrier with a comparatively small influence due to the voltage dependent depletion and funnel region whilst the sensitive area is dominated by diffusion charge collection. Therefore, we assume that the dimensions of the sensitive volume are invariant under voltage scaling. This assumption is supported by measurements performed by Roth [36] which indicate that the area of the sensitive volume is insensitive to bias and the thickness only increases about 10% from half to full bias.

Critical Charge: Carter [32] analyzed in detail electrical model of a resistive load NMOS cell. The critical charge was given by:

$$Q_c = Vh\,Ceff \tag{8}$$

where Vh is the stored high voltage and Ceff is a combination of capacitance associated with the struck node. The stored high voltage will be close to Vdd since the time between cell accesses is much greater then the cell recharging time constant (e.g. 50fF cell capacitance x 1 GΩ = 50us). Note the devices only execute code for a very short time (less then 10 ms) at intervals determined by the patients heart rate (typically, 850 ms). Therefore, the device's memory will spend most of its time unaccessed and at an equilibrium Vh equal to Vdd.

The capacitance, in particular the junction and peripheral drain capacitance are voltage dependent. This dependency was considered by using capacitance equations [37] with process parameter estimates for a typical 1.3µm process. The conversion factor (from eqn (8)) required to convert a critical charge calculated at 5V to an application voltage of 2.8V is 0.59. This is only slightly higher than that which would be calculated without correction (0.56) for voltage-dependent capacitance. Furthermore, the linear dependence between supply voltage and critical charge has been confirmed by SPICE simulations [32].

Heavy Ion Cross-Section Curve Parameters: The previous sections provided two simplifying assumptions for the voltage range of interest; the sensitive volume is independent of voltage and critical charge is a linear function of supply voltage. In order to maintain an invariant sensitive volume with voltage the heavy ion parameters L0 and W (and $\bar{L}$) must scale with voltage in an identical manner to Qc. Thus,

$$Qc = k\,Qc_{test} \quad ; L0 = kL0_{test}; \quad W = kW_{test} \tag{9}$$

where $k = 0.59 \approx \dfrac{Vdd}{Vdd_{test}} = \dfrac{2.8}{5.0}$

This result is consistent with measurements performed by Roth [36] indicating a linear relationship between the median LET, corresponding to 50% of the limiting cross-section, and the bias voltage. The median LET as given by

$$L_{50} = L0 + W\,\log(2)^{1/s} \tag{10}$$

A linear scaling of L0 and W implies a linear scaling of Qc.

4. Estimation of C(Qc,t)

An important assumption in the use of the BGR model is that neutron upsets are treated as energy deposition events occurring at a point. In our case, recoil ranges of the order of a few microns are not much less than the sensitive volume dimensions, in particular the mean sensitive depth of 2.2 µm. Thus, the point deposition assumption requires correction to account for two competing effects. Firstly, strikes inside the sensitive volume that recoil outside and fail to cause upset and, conversely, strikes outside the sensitive volume which recoil inside to generate an upset. In the context of correcting the point deposition assumption, the collection efficiency is then

defined as the ratio of B_{recoil} to B_{point} where B_{recoil} is the total bursts both inside and outside the sensitive volume that may cause upset (accounting for recoil) and B_{point} is the total bursts inside the sensitive volume under point deposition assumption.

A Monte-Carlo simulation was conducted to estimate the collection efficiency as a function of critical charge (minimum recoil length) and mean sensitive depth. Points were randomly sampled in an analysis volume space with dimensions much larger than the sensitive volume. Recoil points were selected at isotropic angles with a range given by noting that the NIE function represents the cumulative distribution function for the charge deposited by recoil nuclei. Having selected a recoil charge based on the NIE distribution the corresponding range and final recoil point is easily calculated. We assume that the charge deposition of recoils may be approximated by a Si ion recoil using the TRIM code [38] since the differences in range of Al, Mg and Si ions are not great for the recoil energies under consideration. A more accurate calculation would consider the proportion of spallation reactions that generate other recoil ions, as well as the charge deposited by light particles such as proton and alpha particles.

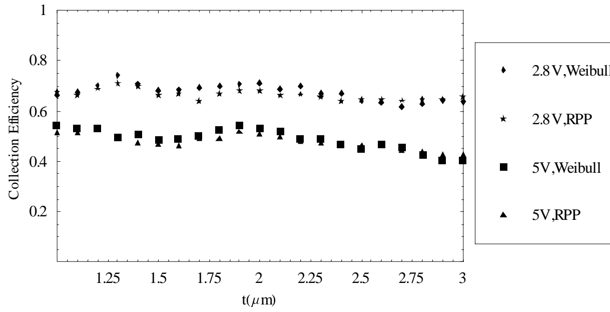

Figure 3: Collection efficiency as a function of mean sensitive depth for two different sensitive volume shapes and two different voltage levels (2.8V and 5V). 10000 samples used in Monte-Carlo analysis.

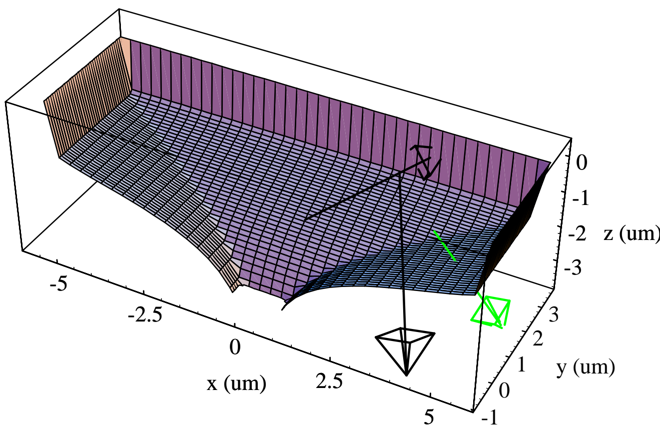

Figure 4: Cross-sectional view of sensitive volume profile and example Monte-Carlo simulation of neutron induced Si recoils. Black arrows denote recoils which generate upsets whilst light colored events do not cause upsets.

The results of the calculation are shown in Figure 3. For comparison purposes, two voltage levels were considered (2.8V and 5V). In addition, the collection efficiency was calculated for two different types of sensitive volume shapes: the heavy ion cross-section derived shape shown in Figure 4 and a rectangular parallelepiped (RPP) of equivalent mean sensitive depth. This analysis explains the success of the RPP approximation with the results indicating that collection efficiency is almost independent of the shape of the sensitive volume provided the RPP has the same mean sensitive depth. As we reduce mean selected depth, the critical charge and corresponding recoil range decrease, which tends to increase collection efficiency. Competing with this effect is the decreasing sensitive depth that tends to reduce collection efficiency. The net result, in Figure 3, is that collection efficiency does not vary with sensitive depth. At lower voltages, the efficiency increases due to the reduced recoil range associated with the lower critical charge.

5. Estimation of dN/dE and F:

An analytic approximation to the differential neutron flux at New York City (NYC) was calculated by Ziegler [42].

$$\frac{dN}{dE_n}(NYC) = 1.5\exp[f(\ln(E))] \quad \text{in n / cm}^2\text{MeVsec} \tag{11}$$

$$\text{where } f(x) = -5.2752 - 2.6043x + 0.5985x^2 - 0.08915x^3 + 0.003694x^4$$

This formula was created by curve fitting to currently available experimental data within the limits 10 to 10000 MeV. However, we require an equation valid down to 1 MeV. Comparison of eqn (11) with Hess' experimental data [39] of the flux from 1-10 MeV and Armstrong's Monte-Carlo calculations [40] in this region indicate that Ziegler's equation is a good approximation even when extended down to 1 MeV.

Now we have a good approximation to the 1-10000 MeV differential neutron flux at NYC but our estimates need to account for the patient distribution of altitude, geomagnetic position and implant time. The correction proceeds by first observing the following relevant characteristics of the study population.

- Latitude varies from Lund (Sweden) at 55.7 degree. to Fort Lauderdale(United States) at 26.1 degree.
- Altitude varies from sea level to 1647 meters (Colorado Springs).
- Device implant times vary considerably from 0 to 1464 days (mean 491, σ 299) due to the wide span of implant dates (from 14-Apr-92 to 8-Feb-96) and a certain small proportion of explants.

The Wilson-Nealy [41] model of 1-10 MeV neutrons in the atmosphere gives the neutron flux in n/cm^{2}sec as a function of altitude (x, the equivalent areal density of the air column in gm/cm^2), geomagnetic position (the corresponding cutoff rigidity R in GV) and the solar activity (Cr, the relative neutron monitor rate). The entire model is given in appendix A due to a typographical error in a previous report [7]. Ziegler[42] provides a convenient relationship to obtain the

areal density of the air column x, in gm/cm^2, from the altitude, H in feet (valid 0<H<40000ft):

$$x = 1033 - (0.03648H) + (4.26 \times 10^{-7} H^2) \tag{12}$$

For simplicity the relative solar activity was assumed constant at 0.87 for all devices; a typical value for the period from 1992 to 1996 [42]. The cutoff rigidity R as a function of geographical location may be determined from a world map of constant vertical rigidity cutoff contours [43] based on the 1 degree latitude and 1 degree longitude tabulations of Smart and Shea [44]. Due to the shape of the earth's magnetic field, the variation of neutron flux is predominantly latitudinal with only a small longitudinal variation.

For each device, we apply the Wilson-Nealy model to calculate the neutron fluence at the patients estimated residing altitude and geographical location. Since the time of implant varies significantly, we then calculate the fluence (n/cm^2) expected for each device. The average flux from 1-10 MeV for the implant population is then given by dividing the sum of the device fluences by the sum of the device operating times. The correction factor required to correct the flux at NYC to the implant population flux is then given by the ratio of their respective Wilson-Nealy estimated fluxes. Note that such a correction assumes that all neutrons in the energy range of 1-10,000 MeV follow the same behavior with respect to altitude, location and solar activity as the 1-10 MeV neutron flux; an assumption considered valid from analysis work performed by Normand and Baker [43]. The method and results are summarized by the following equations:

$$F_{WN(1-10MeV,\text{Implant Pop})} = \frac{\sum_{i=1}^{\#devices} t_i \phi_{1-10MeV}(x(H_i), R_i, 0.87)}{\sum_{i=1}^{\#devices} t_i} \tag{13}$$
$$= 0.00708 \quad n/cm^2/s$$
$$F_{WN(1-10MeV,\text{NYC})} = \phi_{1-10MeV}(x(0), 1.7, 0.87)$$
$$= 0.00686 \quad n/cm^2/s$$

where, t_i is the time from implant to last check up for the ith device and all other variables are as previously defined.

$$\frac{dN}{dE_n}(\text{Implant Pop}) = F_{correction}\frac{dN}{dE_n}(NYC) \tag{14}$$

where $F_{correction} = \frac{F_{WN(1-10MeV,\text{Implant Pop})}}{F_{WN(1-10MeV,\text{NYC})}} = 1.032$

Thus, the average neutron flux received by the implant population is quite well approximated by the flux at New York City with only a small correction required. Integrating eqn (17) from 1-10000 MeV gives the integral flux required for SER calculations (F=0.0129 n/cm^2/s).

6. Estimation of Sf:

Devices implanted within the body are shielded from ground level cosmic radiation by three main factors:

1. Building materials (e.g. concrete, steel, bricks, timber).
2. Body tissue.
3. Device hermetic and internal packaging (e.g. titanium).

An accurate calculation of the effects of these three layers on cosmic ray neutrons is exceedingly complex and beyond the scope of this work. A simplified approach is adopted where we assume that the shielding may be modeled by two distinct shielding environments, a low shield (outdoors) environment, and a shielded (indoor) environment. The shielding factor *Sf* required in the upset rate calculations is then given by

$$Sf = f_{in} S_{in} + (1 - f_{in}) S_{out} \tag{15}$$

where S_{in} and S_{out} are the indoor and outdoor shielding factors and f_{in} is the fraction of time spent by patients with implantable devices indoors. UNSCEAR [10], in dosimetry calculations, uses f_{in} = 0.8 as a typical value for the fraction of time spent indoors.

Ziegler [42] conducted extensive studies of the absorption of cosmic ray neutrons (>50 MeV) under various types of concrete typically found in structural floors and roofs in the United States. The absorption of neutrons in a thickness (t) followed an exponential attenuation with a mean attenuation length (L_n) of 216 g/cm^2 and a typical concrete density(ρ) of 2.45 g/cm^3. The attenuation factor (S) may be expressed as:

$$S = e^{-t\rho/L_n} \tag{16}$$

We assume that the shielding factor is independent of energy, although we note that the neutron cross-section is energy dependent at low to intermediate energies (<100 MeV). We further assume for simplicity that the attenuation length of tissue and device packaging may be approximated by concrete. These assumptions were removed in a previous analysis [15] that produced similar results to this more simplified approach. The thickness and density of each layer in the indoor and outdoor settings are given in Table 3. Applying eqns (15) and (16) gives an average shielding factor, Sf = 0.78.

Table 3.
Implantable device shielding materials

Shielding	Density g/cm^3	Thickness (Indoors)	Thickness (Outdoor)
Building (concrete)	2.45	20 cm	0 cm
Tissue	0.98	10 cm	10 cm
Implanted Device	1.82	3 cm	3 cm
Total Atten. Length	-	64 g/cm^2	15 g/cm^2
Shielding factor	-	0.74	0.93

Average Shielding = 0.74 (0.8) +0.93 (0.2) = 0.78

7. Summary of BGR calculation

Table II summarizes estimates of all variables for the memory cell considered in this study. The close correspondence between the variable depth model and the collection gain model (Table II) indicates that the upset rate is relatively insensitive to interpretation of the heavy ion data. Such a result is attributable to the independence of collection efficiency to sensitive volume shape.

A Monte-Carlo error analysis was used to determine the SER uncertainty. Further analysis of these results and possible errors in the calculation are discussed later in section V.C.

B. Upset Rate by the Neutron/Proton Cross Section Model

The neutron cross-section (NCS) method uses direct measurements of neutron or proton upset cross-section for upset rate estimation. A NSEU cross section is defined as the probability that a neutron of energy En will interact with a semiconductor device and produce an upset in units of cm^2/device. Integrating the product of the NSEU cross section function (σ_{nseu}(En)) and the differential neutron flux (dN/dE) provides the upset rate as follows:

$$SER = \int_{En} \sigma_{nseu}(En)\frac{dN}{dE}dE \tag{17}$$

Typically, proton data is more readily obtained and calculations generally assume that proton and neutron upset rates are approximately equal. Such an assumption is only reasonable for high energies (>100MeV) in which coulomb events are not significant. This calculation is assisted by a two-parameter cross-section model developed by Stapor [45]. Using Harboe-Sorensen's [18] proton cross-section data and a nonlinear fitting routine we obtain:

$$\sigma_{nseu} = \left(\frac{B}{A}\right)^{14}\left[1-\exp(-0.18Y^{0.5})\right]^4, \tag{18}$$

where $Y = \left(\frac{18}{A}\right)^{0.5}(E-A), A = 12.83, B = 11.75$

Using eqn (17) the SER at 5V is 2.2×10^{-12} upsets/bit-hr, in good agreement with the BGR results. Unlike the BGR method, a conversion to the operating voltage of 2.8V is not possible without specific test data. However, we may use a conversion factor (4.6) provided by the ratio of BGR calculations at the different voltages. This gives an SER at 2.8V of 10×10^{-12} upsets/bit-hr.

Table 4.
Theoretical BGR calculation summary

Parameter	Sym	Estimates		Comments
Neutron Flux	F	0.0128 $n/cm^2/s$		Eqn (14)
Shielding Factor	Sf	0.78		Table 3
Heavy Ion Cross-Section Parameters	L0	2.14 $MeVcm^2/mg$		Fit eqn (4) to Figure 2.
	s	4.31		
	W	11 MeV cm^2/mg		
	cs0	0.20 cm^2/device		
Voltage	Vdd	2.8V	5V	
Mean Depth	$\bar{t}$	2.2	2.2	µm
Critical Charge	Qc	0.156	0.262	pC, Eqn (7)
Collect Efficiency	C	0.69	0.51	Monte-Carlo
Neutron Induced Error	NIE	1.05	0.31	$\times 10^{-15}$ $cm^2/\mu m^3$.
Soft Error Rate (Variable depth model, Weibull SV)	SER	4.4	0.95	$\times 10^{-12}$ upset/bit-hr. Eqn (3).
Soft Error Rate (Collection Gain Model , RPP SV)	SER	4.5	1.1	$\times 10^{-12}$ upset/bit-hr. Eqn (5).

Note: All variables shown apply to SER (Weibull SV) calculation.

C. Upset Rate using Monte-Carlo Methods

The Monte-Carlo method is the most accurate approach for SER estimation since the fewest simplifying assumptions are required. Possibly, the most comprehensive modeling package is the SEMM (Soft Error Monte-Carlo modeling program)[46] developed by IBM for chip design. The main disadvantages of this method include program availability and the requirement for detailed circuit layout and process information. Such information is rarely available from manufacturers. For the ICD RAM insufficient data exists for the application of detailed Monte-Carlo methods.

V. Comparison of Field Observations and Theoretical Models

A. Study Population Details

The study population includes 579 devices implanted in-patients in 53 different cities and 10 different countries worldwide. Around 50% of the population are implanted in the US and 25% in Australia.

In all cases, the implanting doctor is required to organize regular follow-up consultations with the patient at intervals of between 3 and 6 months. The protocol for the study population requires parameters and device information to be uploaded via the radio-frequency telemetry link at each consultation. Such information includes details on whether a soft error upset has been detected and corrected.

B. Error Detection, Correction and Logging

In normal operation, the device microprocessor and high frequency oscillator are started when a heart beat is sensed. In the following few milliseconds, the heart rate is calculated and therapy decision algorithms are run. The microprocessor then halts to conserve power until the next heartbeat is sensed. However, a timer also interrupts the microprocessor every hour. This timer activates the error detection algorithm which consists of a simple 16 bit additive checksum performed on the area of memory which is considered read only or executable code. This algorithm adds all memory locations covered by error detection with the sum expected to remain a constant value unless an upset occurs.

If an error is detected a correction algorithm is run. The correction method is a 16 byte Hamming code which can locate any single bit error in up to 64 Kbytes of memory. Following correction, the software is reset and the reset event and cause (memory correction) are logged. This information was obtained by the author.

C. Clinical Single Event Upset Rate

Dividing the total number of SEUs (22) by the sum of the total bit-hours for each model gives an estimate of the SER in upsets/(bit-hr).

$$SER_{field} = 9.3 \begin{cases} 5.5(95\% \, lower) \\ 13.1(95\% \, upper) \end{cases} \times 10^{-12} \, upsets/bithr \tag{19}$$

The number of SEUs in a given time follows a Poisson distribution (similar to radioactive decay). Therefore, the 95% confidence limits on the SER are calculated from the limits (13 and 31) of the expected value of a Poisson distribution with 22 observed counts.

The observed value is about twice the theoretical BGR calculation (using t=2.2μm) and quite close to the proton cross-section method as summarized in Table 5. This discrepancy is well within the statistical uncertainty associated with both the theoretical estimate and the field estimate. A statistical methodology for comparing the observed results with theory is provided in the following section. Differences may also be attributable to inadequacies in the theoretical model including:

1. The calculation is sensitive to the selected value of mean sensitive depth and the assumption that sensitive volume dimensions are independent of voltage. A value of t=0.9μm is required to exactly match theory and clinical results. Such a value also provides a more realistic value for critical charge. Furthermore, this sensitive depth should not be considered too low since it is a mean depth over the entire volume.
2. The model neglects the contribution to charge collection of alpha particle recoil products. Alpha particles emanating from impurities within the IC die are also neglected
3. Uncertainties exist in the BGR function. This function has not been experimentally verified at all energies
4. Inadequate modeling of the diffusion process in the BGR model presented. This problem is well recognized, as evidenced by recent research by Smith and others [47].
5. The calculations have assumed negligible contribution to neutron fluence from aircraft flights. Consideration of average radiation dose in aircraft was made by UNSCEAR [10]. Data for 1989 show that 1.8×10^{12} passenger-kilometers were flown that year which translates into 3×10^{9} passenger-hours aloft. If the population of people that may fly in aircraft is taken as 500 million then the per capita average flight time is 6 hours. Using the Wilson-Nealy model (with R=3.8GV, 8km altitude and 600 km/hr air speed), the increase in neutron flux is a factor of 40, from the 0.007 n/cm^2/s average ground level value. Thus the 6 hours flight time is roughly equivalent to 10 days exposure at ground level. This would introduce a 3% error in our calculation. Even under conservative assumptions, one would expect at most a 20% discrepancy.

Table 5.
Summary of Theoretical and Field SEU

Parameter	Typical	95% CI
SER (BGR t=2.2μm)	4.5×10^{-12} upsets/bit-hr	1.7-11.2
SER (proton x-sect)	10×10^{-12} upsets/bit-hr	
SER (Field)	9.3×10^{-12} upsets/bit-hr	5.5-13.1
Total Upsets(Poisson)	10	3 - 28
Total Upsets(Field)	22	-

D. Poisson Analysis

In order to correctly compare the theoretical and observed results a statistical technique is required that accounts for the uncertainty in both values. Such a method is presented in this section. The number of SEUs, n, in a time, Δt, is known to be Poisson distributed [48] with mean value and variance both equal to $SER\Delta t$. Letting $S = SER$, to simplify notation, the probability function,

$P_1(n, S, \Delta t)$, of n SEUs in a time Δt is given by:

$$P_1(n, S, \Delta t) = \frac{e^{-S\Delta t}(S\Delta t)^n}{n!} \tag{20}$$

From the Monte-Carlo uncertainty analysis of the theoretical section we also have a probability distribution function, $P_2(S)$, for the theoretical SER. The probability, $P(n, \Delta t)$, of n errors in time Δt is then given by:

$$P(n, \Delta t) = \int_{-\infty}^{\infty} P_1(n, S, \Delta t) \; P_2(S) \; dS \tag{21}$$

$$and \sum_{n=0}^{n=\infty} P(n, \Delta t) = 1$$

The effect of using a distribution for the mean SER, (S=SER), as opposed to a fixed value, is to increase the variance of the final probability $P(n, \Delta t)$. If the mean is assumed fixed at the estimated value of 4.5×10^{-12} upsets/(bit hr) and Δt = 284672 days, then between 5 to 16 errors can be expected within 95% probability limits. Conversely, with a SER distribution $P_2(S)$ the 95% probability limits are given by 3 to 28 errors. The 22 upsets observed in the field are well within this bound.

E. Spatial(Geomagnetic position and altitude) Dependence

In this section, we analyze the data to determine if the variation of SER with geomagnetic position and altitude (i.e. estimated neutron flux) is consistent with the Wilson-Nealy model. The method employed involves calculating the neutron flux for each device using the Wilson-Nealy model. The devices are sorted according to the neutron flux and then binned into four flux groups. The high flux group corresponds to devices (or cities) at high altitudes and high latitudes whilst devices in the low flux group are close to sea level at relatively low geomagnetic latitudes. The expected SER for each group involves weighting the total observed SER by the average neutron flux for each group. The neutron fluence for a group is calculated by summing the device fluences and dividing by the

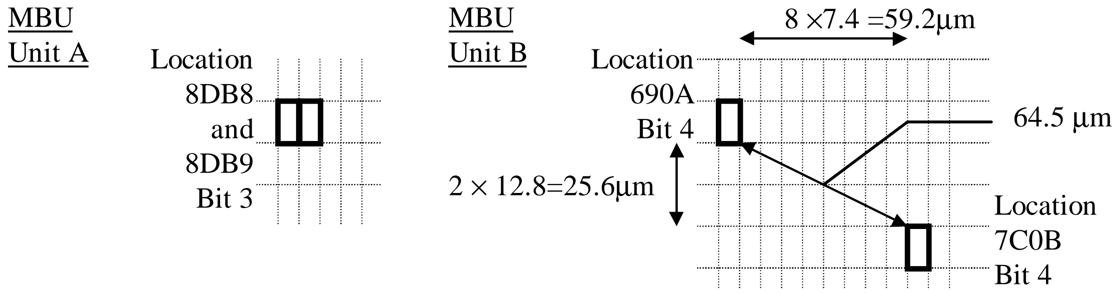

Figure 6: Double bit upset physical locations

sum of the implant times in the group (i.e eqn. 13 applied to the group).

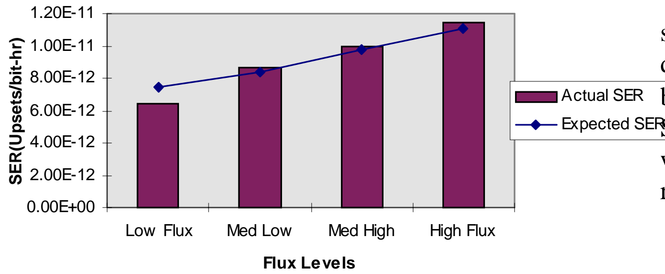

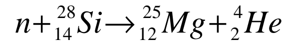

Figure 5. Dependence of SER on flux levels (altitude and rigidity) for the ICD study population. Statistical uncertainty in the observed SER is high since the number of upsets in each category is low.

Figure 5 summarizes the results of a comparison between the expected SER given the Wilson-Nealy flux model and the observed upset rate. Statistical uncertainty in the observed (or actual) SER is high since the number of upsets in each category is low. This prohibits the use of tests of hypothesis techniques to confirm a statistically significant relationship even if we use only two flux levels. Despite the low statistical power, the results thus far are consistent with the Wilson-Nealy model as seen by the trend towards lower upset rates at lower flux levels.

F. Clinical Multiple Event Upset Rate

Two devices in the study population have experienced double bit flip events. We will now examine if these upsets may have originated from secondary neutron cosmic ray upsets. The double bit flip events were characterized by the address bit changes shown in Figure 6.

The logical address bit locations are mapped into physical address space according to the 32K×8 SRAM address map. In this design, identical bit positions (0 to 8) are physically adjacent and there is some scrambling of addresses. Such a layout is common practice as it means that the probability of multiple upsets in the same logical byte is quite low. Double error detecting, single error correcting schemes, which operate on a logical byte basis, then have a low probability of encountering an uncorrectable multiple bit upset.

Inspection of the address map indicates that the double bit upsets of Unit_A are in neighboring cells. This is consistent with diffusion dominated charge sharing between the cells following a neutron strike near both cells. Alternatively, charge sharing between neighboring cells may be generated by a large recoil which intercepts the sensitive volume of both cells.

The physical locations of the upsets of the Unit_B are somewhat different being separated by 2 cells in the y direction and 8 cells in the x direction giving a total distance between upset cells of about 70µm as indicated in Figure 6. Such a pattern is consistent with a neutron strike interacting with the silicon in the following inelastic reaction with the Mg recoil producing one upset and the alpha particle the other:

$$n + {}^{28}_{14}Si \rightarrow {}^{25}_{12}Mg + {}^{4}_{2}He$$

At higher energies, reactions that are more complex may also generate the required alpha emission such as (n, nα) in which both alphas and neutrons are emitted along with the heavy ion recoil. In our case, the alpha particle energy required is around 10MeV (68.5µm) with 2.2 MeV (0.1pC) deposited in the last 8 µm. This will cause upset if the device critical charge is less then 0.1pC.

The occurrence of these MBUs and their consistency with predicted mechanisms of upset via secondary neutron cosmic ray interactions is good supporting evidence that the upset behavior of these static RAMs is attributable to cosmic radiation. The probability (P) of two MBUs occurring so close to each other, within 70 µm, under some other random upset process is very small and is approximately given by:

$$P \approx \left(\frac{\text{Area of 70 mm circle}}{\text{Area cell} \times \text{Number cells}} \right)^2 = 3.4 \times 10^{-7}$$

Thus, the occurrence of two double bit flips within 70 µm is indicative of a non-random process (in terms of relative upset locations) which is well modeled by the mechanisms of double bit upset described.

VI. Conclusion

Overall, the theoretical model presented agrees with observed field results given the low statistics. Furthermore, the physical bit locations of the two observed MBUs are consistent with predicted mechanisms of upset via secondary neutron cosmic ray interactions. These results are evidence that the observed upsets are attributable to secondary neutron cosmic radiation.

Recent evidence suggests that the shape of the heavy ion curve is dominated by intra-cell variation in charge deposition. The collection gain concept of Petersen is incorporated into the BGR method. It was found that the SER calculation,

assuming a variation in collection gain within a cell, is mathematically equivalent to a variation in critical charge across the entire device. We compare calculations for various interpretations of heavy ion data and show that the calculated SER is insensitive to the shape of the sensitive volume. This explains the historically good comparison between experimental results and theory based on RPP geometry.

Implantable devices may be implanted for periods of between 3-8 years before battery depletion requires explant. Improving the longevity of the device drives the design towards low supply voltages since the current consumed by the integrated circuits is the dominant contributor to power consumption (followed by shock power; Devices have the capacity to deliver up to several hundred charges however under clinical conditions a typical patient requires around 10 shocks per year). The low voltage operation greatly increases susceptibility to soft error upsets. Microprocessor based systems in which critical controlling software is in RAM, as opposed to ROM, are especially prone to SEUs. Clearly, an understanding of the soft error rate is vitally important given the high reliability requirements and life-supporting nature of the application.

ACKNOWLEDGMENTS

The authors would like to acknowledge the support of Dr. A. Rosenfeld of the University of Wollongong and Dr. B. Milthorpe of the University of New South Wales and also the assistance of R. Harboe-Sorensen (European Space Agency-Netherlands) and R. Koga (Aerospace Corporation-California) for providing raw heavy ion test data on the 32K × 8 SRAM used in this study.

APPENDIX A-WILSON-NEALY ATMOSPHERIC NEUTRON MODEL

This appendix is presented here to correct for a previous typographical error [43]. The Wilson-Nealy model of 1-10 MeV neutrons in the atmosphere gives the neutron flux, in n/cm^2 sec as a function of altitude (x, the areal density of the air column in g,/cm^2), latitude (the corresponding cutoff rigidity, R, in GV) and the solar activity (C_r, relative neutron monitor rate). Other intermediate terms are defined in [43].

$$\phi_{1-10}(x,R,C_r) = f(R,C_r)e^{-x/\lambda} - F(R,C_r)e^{-x/\Lambda} \quad \text{(A1)}$$

where

$$\phi_{1-10}(x_m,R,C_r) = 0.23 + [1.1 + 0.0167(C_r - 100)]e^{-R^2/81} + [0.991 + 0.051(C_r - 100) + 0.4\,e^{((C_r - 100)/3.73)}]e^{-R^2/12.96} \quad \text{(A2)}$$

$$\phi_{1-10}(250,R,C_r) = 0.17 + [0.787 + 0.035(C_r - 100)]e^{-R^2/25} + [-0.107 - 0.0265(C_r - 100) + 0.612\,e^{((C_r - 100)/3.73)}]e^{-R^2/139.2} \quad \text{(A3)}$$

$$\lambda = 165 + 2R \quad \text{(A4)}$$

$$x_m = 50 + \ln(2000 + e^{-2(C_r - 100)}) \quad \text{(A5)}$$

$$f(R,C_r) = e^{250/\lambda}\phi_{1-10}(250,R,C_r) \quad \text{(A6)}$$

$$\Lambda = \lambda\left(1 - \frac{\phi_{1-10}(x_m,R,C_r)e^{x_m/\lambda}}{f(R,C_r)}\right) \quad \text{(A7)}$$

$$F(R,C_r) = \left(\Lambda/\lambda\right)f(R,C_r)\exp\left(x_m/\Lambda - x_m/\lambda\right) \quad \text{(A8)}$$

REFERENCES

[1] R.J. Myerburg, K.M. Kessler, D. Estes, “Long term survival after pre-hospital cardiac arrest: analysis of outcome during an 8 year study,” *Circulation*, vol. 70, pp. 538-546, 1984.

[2] M. Mirowski, M.M. Mower, W.S. Stawean, “Standby automatic defibrillator, an approach to prevention of sudden cardiac death,” *Arch Int Med*, vol. 29, pp. 158-161, 1970.

[3] F. Rodriguez, A. Filimonov, A. Henning, C. Coughlin, M. Greenberg, “Radiation-induced effects in multiprogrammable pacemakers and implantable defibrillators,” *PACE*, vol. 14 pp. 2143-2153, 1991.

[4] S.K. Souliman and J. Christie, “Pacemaker failure induced by radiotherapy,” *PACE*, vol. 17 270-273, 1994.

[5] T.P Ma and P.V. Dressendorfer(Editors), Ionising Radiation Effects in MOS Devices and Circuits, John Wiley and Sons, 1989.

[6] P.V. Dressendorfer, J.M. Soden, J.J. Harrington, and T.V. Nordstrom, “The Effects of Test Conditions on MOS Radiation-Hardness Results,” *IEEE Trans. Nucl. Sci.,* vol. 28**,** pp. 4281, Dec. 1981.

[7] E.Normand, “Single Event Effects in Avionics,” *IEEE Trans. Nucl. Sci.,*. vol. 43, no. 2**,** pp. 461-474, April 1996.

[8] D. L. Oberg, J. L. Wert, E. Normand, P.P. Majewski and S.A. Wender , "First Observations of Power MOSFET Burnout with High Energy Neutrons,” *IEEE Trans. Nucl. Sci.,*. vol. 43, no. 6**,** pp. 2913, Dec. 1996.

[9] United Nations Scientific Committee on the Effects of Atomic Radiation, Sources and Effects of Ionizing Radiation, 1977 Report to the General Assembly, with Annexes, United Nations, 1977.

[10] United Nations Scientific Committee on the Effects of Atomic Radiation, Sources and Effects of Ionizing Radiation, 1993 Report to the General Assembly, with Annexes, United Nations, 1993.

[11] H.D. Roedler, A. Kaul, “Radiation Absorbed Dose from Medically Administered Radiopharmaceuticals,” p 655-665 in *Biomedical Dosimetry,* IAEA publication, Vienna, 1975.

[12] J. Walter, H. Miller, C.K. Bomford, A Short textbook of Radiotherapy, (Table 10.1),4th Ed, Churchill Livingston,1979.

[13] J.H. Gough, R. Davis, A.J. Stacey, “Radiation Doses delivered to the skin, bone marrow and gonads of patients during cardiac catheterisation and audiocardiography,” *Br. J.Radiol,,* vol. 41**,** pp. 508-518, 1968.

[14] G.H. Fletcher, Textbook of radiotherapy, 2nd Ed, Lea and Febiger., Philadelphia, 1973.

[15] P.D. Bradley, “The effects of ionizing radiation on implantable MOS devices,” Master of Engineering (Biomedical) Thesis, University of New South Wales, July 1996.

[16] F. Masuoka, "Are You Ready for Next Generation Dynamic RAM Chips?,” *IEEE Spectrum*, p. 110, Nov. 1990.

[17] S. Yamamoto, N. Tanimura, K. Nagasawa, S. Meguro, T. Yasui, O. Minato, T. Masuhara, “A 256K CMOS SRAM with variable

impedance data-line loads," *IEEE Journal of Solid-State Circuits,* vol. 20, no. 5, pp. 924-928, Oct. 1985.

[18] R. Harboe-Sorensen, E..J. Daly, L. Adams, C. Underwood, R. Muller, "Observation and prediction of SEU in Hitachi SRAMs in low altitude polar orbits," *IEEE Trans. Nucl. Sci.,* vol. 40, no. 6, pp. 1498-1501, Dec. 1993.

[19] R. Koga, W.A. Kolasinski, J.V. Osborn, J.H. Elder, R. Chitty, "SEU test techniques for 256K static RAMs and comparisons of upsets induced by heavy ions and protons," *IEEE Trans. Nucl. Sci,,* vol. 35, no. 6, pp. 1638-1643, Dec. 1988.

[20] Private Communication: R. Koga (Aerospace Corporation), raw heavy ion test data

[21] Private Communication: R. Harboe-Sorensen (ESA), raw heavy ion and proton test data

[22] E. Normand, "Single-event effects in avionics," *IEEE Trans. Nucl. Sci.*, vol. 43, no. 2, pp. 461-474, April 1996.

[23] J.F. Ziegler, W.A. Lanford, "Effect of Cosmic rays on Computer Memories," *Science*, vol. 20, 776-788, 1979.

[24] R. Silberberg, C.H. Tsao, J.R. Letaw, "Neutron generated single-event upsets in the atmosphere," *IEEE Trans.Nucl.Sci,* vol. 31, pp. 1183-1185, Dec. 1984.

[25] J.R. Letaw, "Burst generation rates in silicon and gallium arsenide from neutron-induced nuclear recoils," *Severn Communications Corporation*, SCC Report 87-02, 1987.

[26] E. Normand, J.L. Wert, W.R. Doherty, D.L. Oberg, P.R. Measel and T.L.Criswell, "Use of PuBe Source to simulate neutron induced single event upsets in static RAMs," *IEEE Trans. Nucl.Sci,* vol. 35, pp. 1523-1528, Dec. 1988.

[27] E. Normand, W.R. Doherty, "Incorporation of ENDF-V Neutron cross-section data for calculating neutron-induced single event upsets," *IEEE Trans. Nucl. .Sci.,* vol. 36, pp. 2349-2355, Dec. 1989.

[28] J.R. Letaw, and E. Normand "Guidelines for predicting Single Event Upsets in Neutron Environments," *IEEE Trans. Nucl. Sci*., vol. 38, pp. 1500, Dec. 1991.

[29] W.R. McKee, et.al. "Cosmic Ray induced upsets as a major contributor to the soft error rate of current and future generation DRAMs," *IEEE Int. Reliability Symp.,* pp. 1-6, 1996.

[30] E.L. Petersen, "Interpretation of Heavy Ion Cross-section Measurements," *IEEE Trans. Nucl. Sci*., vol. 43, no. 3, pp. 952, June 1996.

[31] E.L. Petersen, "Cross-section measurements and upset rate calculations," *IEEE Trans. Nucl. Sci*., vol. 43, no. 6, pp. 2805-2813, Dec. 1996.

[32] P.M. Carter and B.R. Wilkins,``Influences on soft error rates in static RAMs," *IEEE Journal Solid State Circuits,* vol. 22, no. 3, pp. 430-436, 1987.

[33] P.J. McNulty, W.J. Beauvais, D.R. Roth, "Determination of SEU parameters of NMOS and CMOS SRAMs," *IEEE Trans.Nucl. Sci.*, vol. 38, no. 6, pp. 1463-1469, Dec. 1991.

[34] C.Hu, "Alpha Particle Induced field and enhanced collection of carriers," *IEEE Electron Device Letters*, vol. 3, no. 2, pp. .31-34, 1982.

[35] W.G. Abdel-Kader, P.J. McNulty, S. El-Teleaty, J.E. Lynch, and A.N. Khondker, "Estimating the dimensions of the SEU-sensitive volume," *IEEE Trans. Nucl.. Sci.*, vol. 34, no. 6, pp. 1300-1304, Dec. 1987.

[36] D.R. Roth, P.J. McNulty, W.G. Abdel-Kader and L. Strauss, "Monitoring SEU parameters at reduced bias," *IEEE Trans. Nuc. Sci.*, vol. 40, no. 6, pp. 1721-1724, Dec. 1993.

[37] M. Buehler, and R.A. Allen, ``An analytical method for predicting CMOS SRAM upsets with application to asymmetrical memory cells," *IEEE Nuc. Sci.*, vol. 33-6, pp. 1637-1641, Dec. 1986.

[38] J.F. Ziegler, J.P. Biersack, U. Littmark, The stopping and range of ions in solids, New York, Pergamon Press, 1985.

[39] W.N. Hess, H.W. Patterson, R. Wallace and E.L. Chupp, "Cosmic-Ray Neutron Energy Spectrum," *Physical Review,* vol. 116, no. 2, pp. 445-457, 1959.

[40] T.W. Armstrong, K.C. Chandler and J. Barish, "Calculations of Neutron Flux Spectra Induced in the Earth's Atmosphere by Galactic Cosmic Rays," *Journal of Geophysical Research,* vol. 78, no. 16, pp. 2715-2725, 1973.

[41] W. Wilson and J.E. Nealy, ``Model and database for background radiation exposure of high altitude aircraft," in *Proceedings of the topical meeting on new horizons in radiation protection and shielding-American Nuclear society,*1992.

[42] J.F. Ziegler "Terrestrial cosmic rays," *IBM J. Res. Develop.*, vol. 40, no. 1, pp.19-39, Jan. 1996.

[43] E. Normand and T.J. Baker, "Altitude and latitude variations in avionics SEU and atmospheric neutron flux," *IEEE Trans. Nucl. Sci*., vol. 40, no. 6, pp. 1484, Dec. 1993.

[44] D.F. Smart and M.A. Shea, ``The distribution of galactic cosmic rays and solar particles to aircraft altitudes," in *Proceedings of the topical meeting on new horizons in radiation protection and shielding-American Nuclear society,*1992.

[45] W..J. Stapor, ``Two parameter Bendel model calculations for predicting proton induced latchup," *IEEE Trans. Nucl. Sci.,* vol. 37, no. 6, pp. 1966, Dec. 1990.

[46] P.C. Murley and G.R. Srinivasan, ``Soft Error Monte-Carlo modeling program, SEMM," *IBM J. Res. Develop,* vol. 40, no. 1, pp. 109-118, Jan. 1996.

[47] E.C. Smith, E.G. Stassinopoulos, G. Brucker, C.M. Seidlick, "Application of a diffusion model to SEE Cross sections of modern devices," *IEEE Trans..Nucl. Sci.*, vol. 42, no. 6, pp. 772-1779, Dec. 1995.

[48] Browning, R. Koga, W. Kolanski, ``Single event upset rate estimates for a 16K CMOS SRAM," *IEEE Trans. Nucl. Sci.*, vol. 32, no. 6, pp. 4137-4139, Dec. 1985.